FOURTEENTH EUROPEAN ROTORCRAFT FORUM

Paper No. 20

COMPUTATION OF VISCOUS AERODYNAMIC CHARACTERISTICS OF 2-D AIRFOILS FOR HELICOPTER APPLICATIONS

by R. Houwink, J.A. van Egmond and P.A. van Gelder

National Aerospace Laboratory NLR,
Amsterdam, The Netherlands.

20-23 September 1988

MILANO, ITALY

ASSOZIAZIONE INDUSTRIE AEROSPAZIALI
ASSOZIAZIONE ITALIANA DI AERONAUTICA ED ASTRONAUTICA

COMPUTATION OF VISCOUS AERODYNAMIC CHARACTERISTICS OF 2-D AIRFOILS FOR HELICOPTER APPLICATIONS

by R. Houwink, J.A. van Egmond and P.A. van Gelder

National Aerospace Laboratory NLR,
Amsterdam, The Netherlands.

Summary.

An outline is presented of a computer code, used for the prediction of quasi-steady and unsteady aerodynamic characteristics of rotor blade sections in oscillatory and linear pitching motions. The code, named ULTRAN-V, is based on unsteady transonic small perturbation theory, coupled in strong interaction with an usteady version of Green's lag-entrainment method for a turbulent boundary layer. Results are compared with experimental data for the NACA0012 airfoil and for actual rotor blade sections. Provided that the stall behaviour is not dominated by leading edge separation, a reasonably accurate prediction of quasi-steady and unsteady airfoil characteristics up to stall conditions is obtained.

1. Introduction

An important aspect of rotor aerodynamics is the influence of viscous phenomena on rotor blade loading. A theoretical prediction of these effects is difficult due to the three-dimensional, unsteady and periodic subsonic-/transonic nature of the flow. In practice these effects are often accounted for in an approximate way using two-dimensional viscous blade section data, in combination with 3-D inviscid rotor aerodynamics prediction methods. For aerodynamic rotor design and analysis there is a strong need for efficient computational methods to predict these 2-D sectional properties. At separated flow conditions, methods based on the Navier-Stokes equations are capable to give the most realistic prediction of these properties. Although the application of such methods on a routine basis is becoming increasingly attractive in view of the growing performance of nowadays computers, there still remains a continuing interest in less sophisticated computer codes which can generate relatively quick, inexpensive solutions, usually at the price of lower accuracy. Typical examples are computer codes based on transonic small perturbation (TSP) theory coupled with boundary layer methods, which are efficient tools to predict boundary layer effects on unsteady airloads (Refs. 1 to 4).

The present paper deals with the applicability of a computer code in the latter category, named ULTRAN-V.* The code has been applied extensively to predict steady and unsteady aerodynamic characteristics of airfoil sections, including maximum lift. Recently also experience has been obtained in European industrial helicopter projects. The code is based on a 2-D unsteady TSP method and an integral method for the unsteady turbulent boundary layer. A strong interaction coupling procedure allows the computation of attached as well as separated flow.

*) The computer code has been developed under contract with the Netherlands Agency for Aerospace Research NIVR.

The present version of the code has been developed at NLR in various stages, starting from the NASA-Ames code LTRAN2 (Ref. 5) which was based on low frequency TSP theory. The aim of this development originally was to improve the prediction of unsteady airloads on oscillating transonic wing sections for aeroelastic analyses, by taking into account boundary layer effects. Results of an earlier version (LTRAN2-NLR) of the present code with Green's lag-entrainment method for the steady turbulent boundary layer (Ref. 6) were reported in Refs. 7 to 9.
Besides an improved prediction of unsteady airloads in attached flow, the code also appeared to give reasonably accurate predictions of maximum lift (Refs. 9, 10). In order to improve the predictions of strong unsteady viscous effects, the present version of the code has been developed which includes a fully unsteady model for the inviscid flow and the turbulent boundary layer.

In the present paper an outline is given of the ULTRAN-V code. The applicability and limitations of the code for rotor blade sections are demonstrated by examples of computed subsonic and transonic, attached and separated flow characteristics of 2-D airfoils at constant pitch rate and in harmonic pitching motion. Computed quasi-steady and unsteady airloads, including maximum lift coefficients, are compared with experimental data for the NACA0012 airfoil (AGARD test cases) and for realistic rotor blade sections. Because modifications to obtain a fully time-accurate coupling procedure in the ULTRAN-V code were not completed yet at the time of the present applications, the results presented here have been computed using the semi-time-accurate version.

2. Computational method.

2.1. Inviscid outer flow

The ULTRAN-V code computes the development of two-dimensional unsteady subsonic or transonic flow about an airfoil in steady or unsteady motion. The inviscid outer flow method is a modified version of the NASA-Ames code LTRAN2 (Ref. 5). The present version is based on the unsteady transonic small perturbation equation for the velocity potential, which is solved on a rectangular grid using an Alternating Direction Implicit method. The flow equation is given by:

$$\{[1-M_\infty^2-(\gamma^*+1)M_\infty^2\varphi_x]\varphi_x\}_x+\varphi_{zz}-2M_\infty^2\varphi_{xt}-M_\infty^2\varphi_{tt} = 0 \qquad (1)$$

where $\gamma^*=2-(2-\gamma)M_\infty^2$. The boundary conditions on airfoil $z= h(x,t)$ and wake, taking into account the displacement thickness effect $d=\delta^*(x,t)$, are given by:

airfoil: $$\varphi_z = h_x + h_t + d_x + d_t \qquad (2)$$

wake : $$\Delta_z\varphi_z = d_x + d_t \qquad (3)$$

$$\Delta_z(\varphi_x + \varphi_t) = 0 \qquad (4)$$

Condition (4) results from the requirement that the linearized pressure coefficient is continuous accross the wake. Boundary conditions upstream and at upper and lower edges of the computational grid are specified by prescribing the perturbation potential distribution due to a vortex at the quarter chord point, having the circulation G of the airfoil:

$$\varphi = \varphi(G) \tag{5}$$

At the downstream boundary the condition is

$$\varphi_x = 0 \tag{6}$$

Instantaneous lift and moment (positive nose-up) coeffients C_l and C_m are computed by integration of the instantaneous pressure coefficient C_p over the airfoil surface. C_p is determined using the full potential expression, neglecting the contribution of the φ_z term. This choice has appeared to give the best agreement of inviscid results with full potential theory. The drag coefficient C_d is derived from the boundary layer momentum thickness in the far wake. At transonic flow conditions, C_d is increased by the shock wave drag. This drag is determined approximately, using normal shock relations for the local Mach numbers upstream of the shock points. The finite difference approximations and the numerical solution technique are largely similar to that of the original LTRAN2 code. Main modifications concern the addition of the φ_{tt} term in Eq.(1) following Ref.(11), implementation of the Engquist-Osher sonic and shock-point operators following Ref.(12) and modification of the z-sweeps of the ADI method. In the ADI method, at each time step a preliminary solution $\varphi(x)$ is computed in x-sweeps for all grid lines z= constant, using the "old" boundary conditions of the previous time level. In the subsequent z-sweeps the final solution $\varphi(z)$ is computed for all lines x= constant in a downstream marching procedure, using the boundary conditions valid for the new time level. For each streamwise station, a z-sweep involves the solution of a tridiagonal system of linear equations for the new potential $\varphi(z)$. In the ULTRAN-V code the z-sweep is reorganized such that it can be interrupted on airfoil surface or wake. In such a point the z-sweep yields coefficients a and b of a linear relation between the new potential and the local boundary condition:

$$\varphi = a + b(h_x + h_t + \delta^*_x + \delta^*_t) \tag{7}$$

In case of inviscid flow (δ^*=0) or weak interaction coupling procedure (δ^* computed at a previous time level) the right hand side of Eq.(7) is known, and the z-sweep can be completed. In the strong interaction procedure, however, φ and δ^* have to be computed by simultaneous solution of Eq.(7) and the boundary layer equations (Section 2.2). To prepare for this solution. Eq.(7) is recast in the following form using finite difference approximations to the velocity gradient $u_x = \varphi_{xx}$ and to the derivatives δ^*_x and δ^*_t:

$$u_x = c_1 + c_2 \cdot \delta^*_x \tag{8}$$

This equation has the same form as used for the steady bounary layer. It can be considered as an inviscid "interaction law", which is needed to allow integration of the boundary layer equations wihout numerical problems at separation, discussed in the next section.
After computation of u_x and δ^*, Eq.(7) can be solved for φ and the z-sweep is completed like in inciscid or weak interaction computations.

2.2 Boundary layer and wake.

The initial part of the boundary layer is computed using a compressible flow version of the laminar boundary layer method of Thwaites (Ref.12) and the transition prediction method of Granville (Ref.13). The turbulent boundary layer and wake are modeled according to a modified version of Green's lag-entrainment method. The modifications concern extension of the shape factor relation $H_1(\bar{H})$ to separated flow (Ref.7), the strong interaction formulation and the unsteady formulation of the turbulent boundary layer. The objective of the latter modification was to improve the prediction of the bounary layer effect at unsteady separated flow conditions. The capability of such strongly interacting inviscid-flow/unsteady boundary layer methods has been demonstrated by Le Balleur (Ref.1). The turbulent boundary layer equations used in the ULTRAN-V code can be written in terms of entrainment coefficient C_E, momentum thickness Θ, displacement thickness δ^*, skin friction coefficient C_f and shape factors H_1 and $\bar{H}$ as follows (dimensional quantities scaled by chord and free stream quantities):

$$\text{entrainment} : \frac{1}{\rho u}\left[\rho(H_1 + \bar{H})\Theta\right]_t + \frac{1}{\rho u}\left(\rho u H_1 \Theta\right)_x - C_E = 0 \tag{9}$$

$$\text{momentum} : \frac{1}{\rho u}\left(\rho \bar{H}\Theta\right)_t + \frac{1}{\rho u^2}\left(\rho u^2 \Theta\right)_x + \frac{\delta^*}{u}\left(\frac{1}{u} u_t + u_x\right) - \frac{C_f}{2} = 0 \tag{10}$$

$$\text{lag equation:} \frac{1}{u}(C_E)_t + (C_E)_x - f_5 - f_6\left(\frac{1}{u} u_t + u_x\right) = 0 \tag{11}$$

Here u and ρ are velocity and density at the edge of the boundary layer. The unsteady entrainment and momentum equations were derived in a straightforward way, starting from the 2-D unsteady compressible turbulent boundary layer equations. Apart from the time derivatives the above equations correspond to Green's lag-entrainment method.
For the closure relations the steady formulation was maintained. In the steady method, prior to integration, Eqs (9) to (11) without time derivatives were recast in the following form (Ref.3):

$$\delta^*_x = f_1 + f_2\, u_x \tag{12}$$

$$\Theta_x = f_3 + f_4\, u_x \tag{13}$$

$$(C_E)_x = f_5 + f_6\, u_x \tag{14}$$

The coefficients f_1 to f_6 are functions of boundary layer and edge flow quantities, which have to be determined bij integration of Eqs.(12) to (14). In the steady method a 2nd order accurate Runge-Kutta method is used. Because this steady formulation appeared to be very well suited for a strong interaction procedure, for the present unsteady method the same form (12) to (14) was derived from Eqs.(9) to (11). In addition to the closure relations and a one-dimensional isentropic flow relation for the density, this also required elimination of the time derivatives using finite difference approximations to time and space derivatives. As a result the integration method for the steady boundary layer could be maintained.

In the case of attached flow, Eqs. (12) to (14) can be integrated on airfoil and wake directly for prescribed velocity distribution. However, near separation the coefficient f_2 in Eq. (12) becomes infinite and changes sign, which inevitably leads to a breakdown of direct integration. In order to avoid this numerical problem, Eq.(12) is recast in the following form:

$$u_x = d_1 + d_2 \cdot \delta^*_x \qquad (15)$$

Here $d_2 = 1/f_2$ becomes zero near separation. By adding the interaction law Eq.(8), δ^*_x and u_x can be computed simultaneously, provided that $c_2 \# d_2$. In practice this conditon appears to be guaranteed in general for attached and separated flow using a central difference approximation to u_x.

2.3 Coupling procedure and iteration process.

The coupling procedure and iteration process of the ULTRAN-V code are shown schematically in Fig.1. At each time step a weak interaction coupling procedure is applied for the initial laminar and turbulent part of the boundary layer up to a station x_{si}. Downstream of this station the strong interaction procedure is applied for turbulent boundary layer and wake.
Before beginning a new time step, the initial part of the boundary layer upstream of x_{si} is computed in direct mode, for given velocity distribution from the previous time level. After performing th x-sweeps, for the subsequent z-sweeps up to the station x_{si} the boundary conditions are updated using the displacement thickness distribution computed in direct mode:

$$d^{n+1}_{x,t} = r\delta^{*\,n}_{x,t} + (1-r)\, d^{\,n}_{x,t} \qquad (16)$$

Here r is a relaxation factor which in the present applications has the value r=0.5, and n indicates the previous time level.
Downstream of x_{si} the displacement thickness is considered as unknown, and the strong-interaction procedure is carried out. By simultaneous solution of Eqs.(8) and (15), the singularity encountered in direct mode is now generally avoided. Solution of Eqs.(8) and (15) and subsequent integration of the boundary layer equations requires an iteration process, in which the coefficients d_1 and d_2 are updated until convergence. Finally the potential φ at the new time level is computed using Eq.(7), and the z-sweep is continued until the next streamwise step. In the present computations, a relaxation factor r=0.5 has also been applied in the strong-interaction region. Because the z-sweeps are carried out in a downstream marching process, the central difference approximation to u_x contains an "old" downstream value of the potential. As a result the flow solution is not fully time-accurate, unless an additional iteration process (Fig.1) is carried out to update the downstream potential and, consequently, the coefficient c_1 in Eq.(8). At present the fully time-accurate iteration process is being completed and tested. In the present computations this option has not yet been applied. Both due to the relaxation factor r=0.5 and the non-iterative z-sweeps the results presented in the following sections are not fully time-accurate. However, because the essential effects of the unsteady boundary layer are modeled, dynamic effects can be expected to be predicted more accurately than using the steady boundary layer model.

The above coupling process allows the computation of attached and separated flow in a natural way, without any special modeling of strong viscous/inviscid interaction at shock-waves, trailing edge, and separation or reattachment points. Taking into account the effect of the boundary layer and wake in the present computations increases the computational effort by about 50% as compared to an inviscid computation. In fully time accurate mode this increase will be considerably larger.

3. Computations and results.

3.1. NACA0012 airfoil (AGARD test cases).

In order to verify the applicability of the present method for typical rotor conditions, two types of AGARD test cases (Ref.15) were selected. Experimental data were obtained by ARA. The first type is an oscillatory piching motion about 0.25 chord, at a reduced frequency based on semi-chord $k=0.081$. Amplitudes are $\delta = 2.44$ and 5 deg about a mean incidence of $\delta = 4.86$ deg. The nominal Mach number is $M_\infty=0.57$ and Reynolds number is $Re_m=4.6*10^6$ based on chord length. The second type is a linear pitching motion over an incidence range from 0 to 15 deg approximately. In addition to pitch rates of 425 and 1380 deg/s (AGARD cases CT 7 and 8) also an almost quasi-steady motion was considered.

The oscillatory pitching motions were computed during four cycles of motion, at the effective Mach number $M_\infty=0.6$ and Reynolds nuber $Re=4.8*10^6$. A downstream limit of transition was prescribed at 0.1 chord. All computations were carried out on a 79*58 grid with 2*33 points on the airfoil, and taking 120 time steps per cycle. In all cases the unsteady boundary layer model was used on the airfoil; in the wake the steady model was used. As discussed in section 2.2 in all cases the z-sweeps of the ADI method were carried out only once per time step.

A comparison of the computed lift and moment coefficients with experimental data is shown in Fig.2. In both cases the lift coefficient is rather well predicted. At the lower amplitude the upper sharp edge in the C_ℓ loop is associated with the temporary presence of a small region of separated flow at the foot of the shock wave, as indicated by the skin friction distribution not shown here. Taking into account the formal limitations of the code, the realistic prediction of the dynamic stall loop at the larger amplitude is surprising. The predicted moment coefficients are somewhat less accurate, but show a rather similar behavior in particular at the lower amplitude. The qualitative disagreement in C_m near the maximum angle of attack is due probably to the effect of unsteady vortex flow, which is not modeled in the present method. Corresponding distributions of computed pressure, skin friction coefficient and displacement thickness during the fourth cycle are shown in Fig.3 for the larger amplitude. The pressure distributions show the development of a shock wave, causing flow separation at the larger angles of attack. In the down stroke the flow reattaches and becomes subsonic again. The skin friction coefficient C_f indicates the development of a shock-induced separation bubble, followed by a second separation at the trailing edge. In the down stroke, the flow reattaches suddenly, which explains the temporarily constant lift coefficient at decreasing angle of attack (Fig.2). With the development of the flow separation, the displacement thickness shows a strong increase until a maximum of 9% chord at the beginning of the down stroke. The jump at the shock wave is clearly visible.

The computations for the linear ramp motions were carried out at the same flow conditions, using the same configuration of the computer code. The quasi-steady motion was approximated by an unsteady motion of 100 deg/s. In all cases the same time step size of 0.2 chord was take, which gives a consistent basis for comparison of the ramp motion results.

The computed lift and moment coefficients are shown in Fig.4, in comparison with the ARA experimental data. The development of the lift coefficient with increasing incidence is predicted reasonably well up to and including maximum lift. The effect of rotational velocity, which yields a higher maximum lift is also well predicted. At higher angles of attack, however, the computed lift quickly decreases significantly below the experimental values.

The moment coefficients are predicted with less accuracy, in particular at the higher pitch rate. More insight is obtained by comparing the time history of computed and measured pressure distributions, shown in Fig.5. The development of measured pressures up to about 9 deg is approximately similar to the computed results up to about 11 deg. The predicted downstream motion of the shock wave seems to be retarded, and the leading edge pressures are reaching too high values compared to the experimental data. The latter observation is rather common for TSP results. At higher angles of attack, the shock wave is forced upstream due to the interaction with the separating boundary layer. The measured upper surface pressures show a wavy behavior, which may be associated with the effect of vortices separating from the leading edge, or with secondary shock waves. These phenomena are not predicted by the present method. At maximum angle of attack the flow is fully separated, and the pressure distributions are rather similar, except for a difference in level on the upper side. In contrast, the lower surface pressures are predicted very well for the complete range of incidences.

The above observations indicate that the present method can be a useful tool to predict unsteady lift at separated flow conditions. The prediction of moment coefficients and pressure distributons in the present examples, however, is less accurate. This indicates a limitation of the present theory for the prediction of leading edge separation. It is not known, to what extent wall interference effects contribute to the observed (dis)agreement between experimental and theoretical data.

3.2. Quasi-steady characteristics of blade sections

In this section some results are presented of the application to a representative family of helicopter blade sections. In order to calculate 2D-lift curves a quasi-steady approach has been used, in which unsteady terms in boundary layer and boundary conditions were switched off. The calculation procedure starts with a 2D-profile at a negative angle of attack and rotates at a constant (small) pitch rate to its maximum value well beyond $C_{\ell max}$. This procedure uses less computer time, as compared to steady calculations, whereas the effect on maximum lift is rather small. It is possible to obtain "steady" values by extrapolation using different pitch rates.

In order to categorize helicopter profiles, use is quite often made of the maximum-lift coefficient at $M_\infty = 0.40$ (which is an important parameter for maneuver conditions), versus the drag divergence Mach number (M_{dd}, which is an important parameter with respect to forward flight conditions at high speeds). When characteristics of various helicopter blade sections are compared, use is quite often made of data obtained from different windtunnel tests.

With the ULTRAN-V code the possibility exists to create a theoretical data base for various airfoils, without differences often present in windtunnel conditions (Reynolds numbers, wall interference effects).

In Figure 6 the calculated lift-curves are presented for a "family" of profiles in comparison with measured values for C_{lmax}. This "family" of profiles has been developed for helicopter applications by Aerospatiale and ONERA, and the difference between these profiles (OA 309, OA 312 and OA 313) is mainly a thickness variation. A fairly good agreement exists between the predicted C_{lmax} and test-data.
For the same profiles drag at zero lift conditions is presented, in Fig. 7 as a function of Mach number. From the drag curves M_{dd} can be obtained using the definition that M_{dd} is the Mach number for which $dC_d/dM_\infty = 0.1$. Again the windtunnel results are added, indicating a good prediction.

3.2. Unsteady characteristics of RAE 9645 airfoil

RAE 9645 is one of the BERP main rotor blade airfoil sections (Ref.16). It represents an advanced high performance blade section. The thickness/chord ratio is 12%. The airfoil exhibits very good low speed high lift characteristics and reasonable high Mach number performances. Dynamic tests have been performed at ARA (Bedford) and test results have been reported by P.G. Wilby (Ref.17). Ramp motion characteristics have been calculated with the ULTRAN-V code and some of the low speed results will be discussed below.

For $M_\infty = 0.3$ calculated and measured results are compared in figures 8, 9 and 10. Figure 8 compares C_l-Alpha and C_m-Alpha curves at low pitch rate, and reasonable correlation is found up to the point of gross flow separation. Results at high pitch rate are shown in Fig. 9. In this case the computations fail to predict the strong overshoot in C_l, probably because vortices separating from the leading edge are not modeled in the present theory. In Ref.(16) it is concluded that, most probably, the RAE 9645 stall behavior at low pitch rates is triggered by a rear separation while at a pitch rate of 1200 deg/sec this rear separation is suppressed and the leading edge pressure distribution becomes the stall trigger. Finally Fig.(10) compares predicted and measured angles for moment break as function of pitch rates and a reasonable correlation is found for moderate pitch rates.

From this example it is concluded that dynamic airfoil characteristics are reasonably well predicted as long as rear separation triggers the stall behavior. Due to the nature of the TSP method and due to the lack of modeling vortex shedding effects, correlation becomes increasingly poor for conditions at which leading edge separation determines the unsteady characteristics. At the same time the RAE 9645 results show that rear separation might play a significant role in the dynamic behaviour of advanced rotor blad sections. Then the application of the ULTRAN-V code may be useful to support interpretation of airfoil characteristics and to obtain insight into (some of) the flow phenomena.

4. Concluding remarks.

Using unsteady transonic small perturbation theory coupled in strong interaction with an unsteady boundary layer method, an efficient prediction of subsonic and transonic aerodynamic characteristics can be obtained for rotor blade sections in quasi-steady and unsteady motion.

The predicted effects of pitch rate, amplitude, and airfoil thickness agree reasonably well with experimental data provided that incipient stall is not dominated by leading edge separation. Further investigation is neccessary to establisch the accuracy of the fully time accurate version of the present code.

Because the applications considered are well outside the formal range of applicability of the theory used, the accuracy can be expected to depend on the type of airfoil and flow conditions. Consequently, interpretation of results for new airfoils should preferably be supported by verification of the code for comparable known airfoil and flow conditions.

Acknowledgment

The authors wish to thank RAE and Mr. F.J. Perry from Westland Helicopters Ltd. for contributing to the present analyses of RAE 9645 data. Also they wish to express their appreciation to Aerospatiale and ONERA for the possibility to use the OA profile data.

References

1) Le Balleur, J.C., Girodroux-Lavigne, P.: "A viscous-inviscid interaction method for computing unsteady transonic separation". Numerical and Physical Aspects of Aerodynamic Flows III. Ed T. Cebeci, Springer - Verlag, 1986

2) Desopper, A., and Grenon, R.: "Couplage fluide parfait fluide visqueux en écoulement instationnaire bidimensionnel incompressible et transsonique". AGARD -CP-291, paper 5, 1981.

3) Houwink, R.: "Unsteady airload computations for airfoils oscillating in attached and separated compressible flow". AGARD CP 386, paper 14 (1985). Also: NLR MP 85040 U (1985)

4) Howlett, J.T., Bland, S.R.: "Calculation of Viscons Effects on Transonic Flow for Oscillating Airfoils and Comparisons With Experiment". NASA TP 2731, 1987.

5) Ballhaus; W.F. and Goorjian, P.M.: Implicit finite difference computations of unsteady transonic flows about airfoils, including the treatment of irregular shock wave motion". AIAA paper 77-205,1977.

6) Green, J.E., Weeks, D.J. and Brooman, J.W.P.: "Prediction of turbulent bounday layers and wakes in compressible flow by a lag-entrainment method". ARC R and M No. 3791, 1973.

7) Houwink, R,: "Results of a new version of the LTRAN2-NLR code (LTRANV) for unsteady viscous transonic flow computations". NLR TR 81078 U (July 1981).

8) Houwink, R. and Veldman, A.E.P.: "Steady and unsteady separated flow computations for transonic airfoils". AIAA paper 84-1618, 1984. Also: NLR MP 84028 U.

9) Houwink, R. "Computations of separated subsonic and transonic flow about airfoils in unsteady motion". Numerical and Physical Aspects of Aerodynamic Flow III, ed. T. Cebeci, Springer, 1986. Also: NLR MP 84094 U (1984).

10) Voogt, N., Mol, W.J.A., Stout, J. and Volkers, D.F.: "CFD Applications in design and analysis of the Fokker 50 and Fokker 100" AGARD-CPP-437, Paper 19, 1988.

11) Hessenius, K.A. and Goorjian, P.M.: " Validation of LTRAN2-HI by Comparison with Unsteady Transonic Experiment" AIAA Journal, Vol 20, No. 5, May 1982, pp. 731-732.

12) Goorjian, P.M., van Buskirk, R.: "Implicit Calculations of Transonic Flows Using Monotone Methods". AIAA paper 81-0331,1981.

13) Rott, N., Crabtree, L.F.: " Simplified laminar boundary layer calcuations for bodies of revolution and for yawed wings". Journal of the Aeronautical Sciences, August 1952.

14) Granville, P.S.: "The calculation of the viscous drag of bodies of revolution". David Taylor Model Basin Rep. 849, 1953.

15) AGARD: Compendium of Unsteady Aerodynamic Measurements. AGARD R-702, data set 3, 1982.

16) Perry, F.J.: "Aerodynamics of the Helicopter World Speed Record" 43rd Annual National Forum of the American Helicopter Society, May 1987.

17) Wilby, P.G.: "An experimental investigation of the influence of a range of aerofoil design features on dynamic stall onset" 10th European Rotorcraft Forum, paper 2, The Hague, 1984.

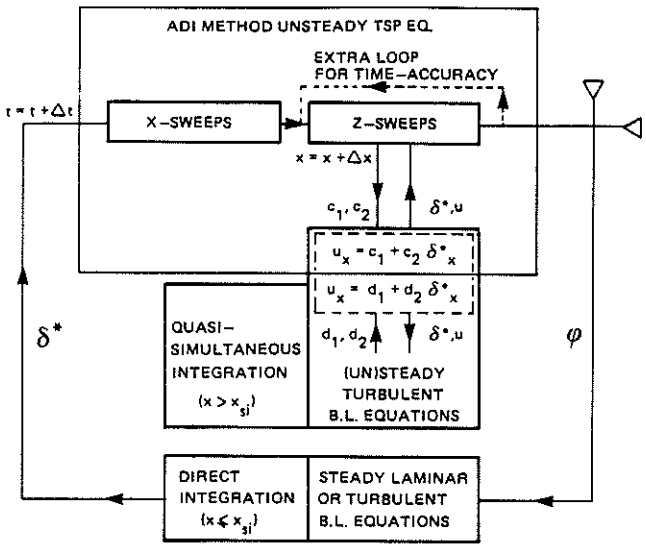

Fig. 1 Organization of unsteady flow computation in ULTRAN-V code

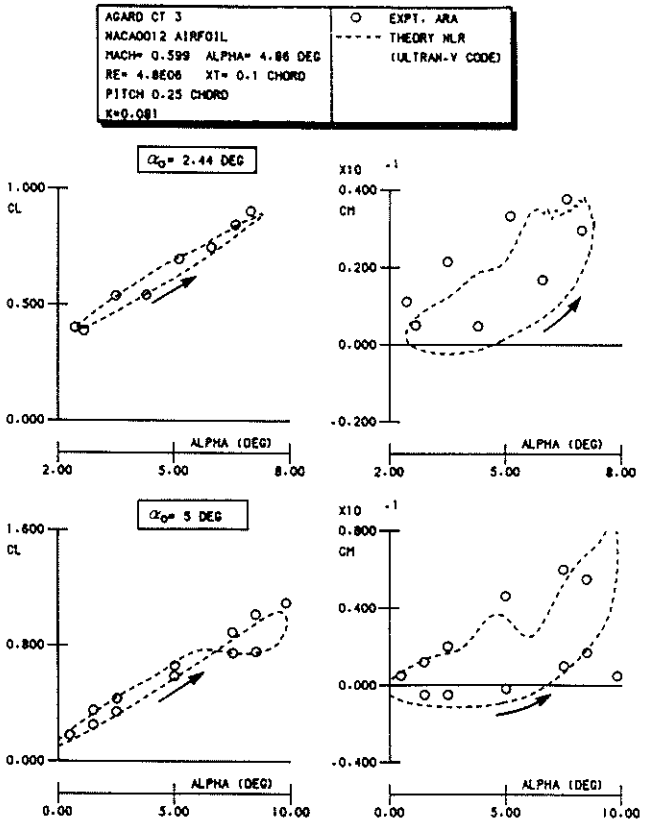

Fig. 2 Lift and moment coefficients during oscillatory pitching motion showing effect of amplitude

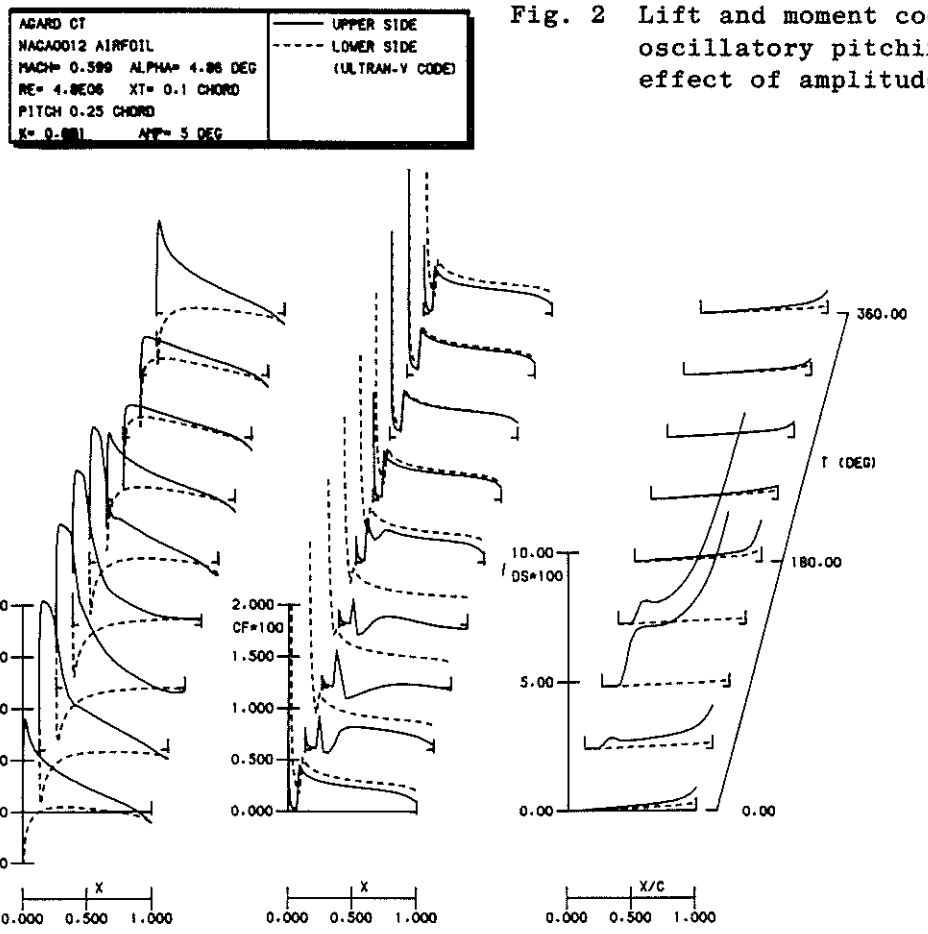

Fig. 3 Distributions of pressure, skin friction coefficient and displacement thickness during 4th cycle of oscillation

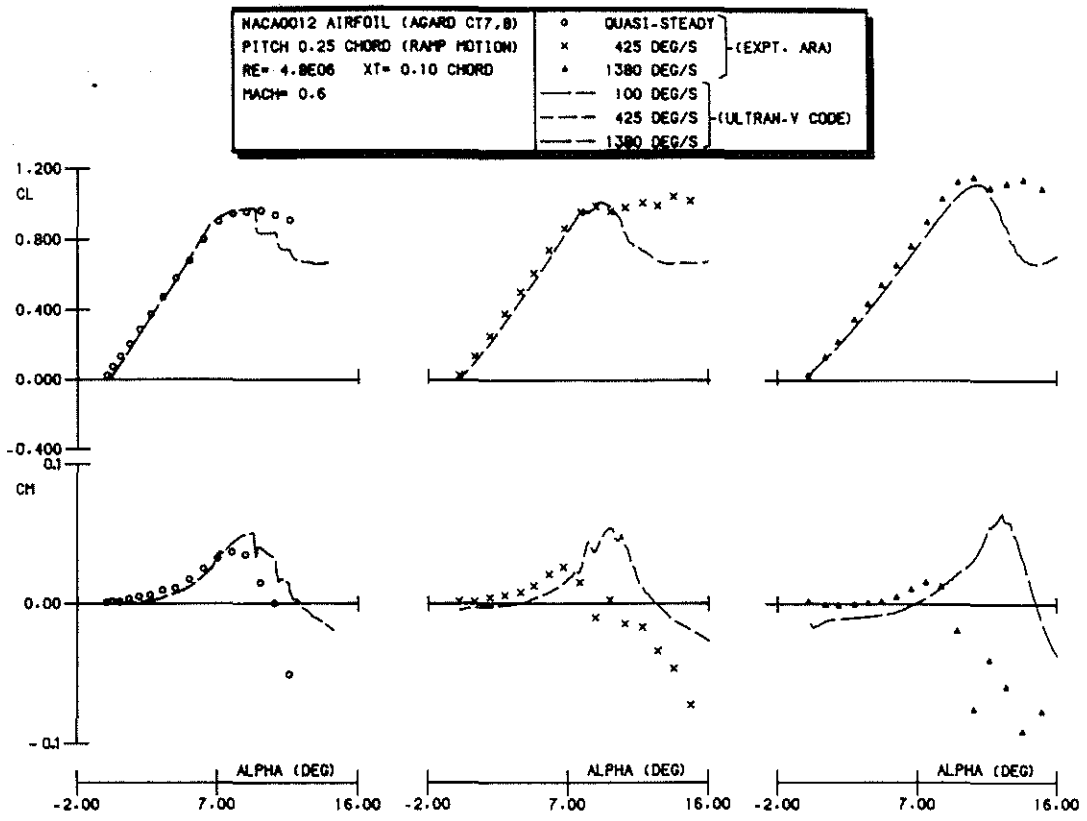

Fig. 4 Unsteady lift and moment coefficients showing effect of rotation speed

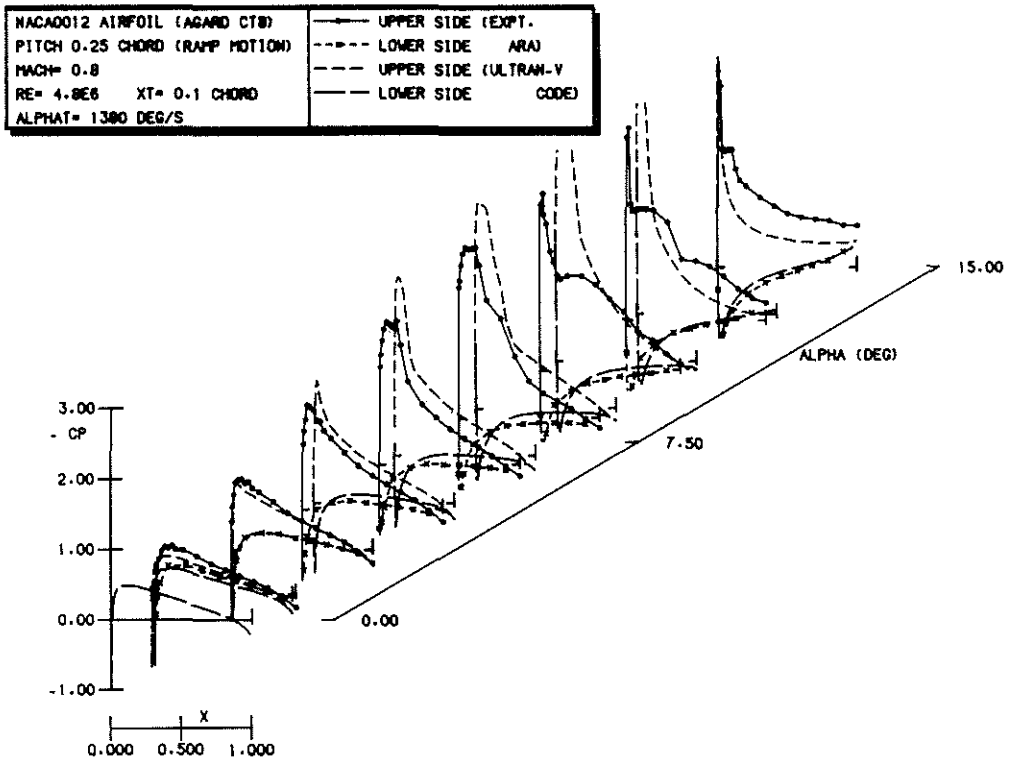

Fig. 5 Unsteady pressure distributions during ramp ramp motion of 1380 deg/s

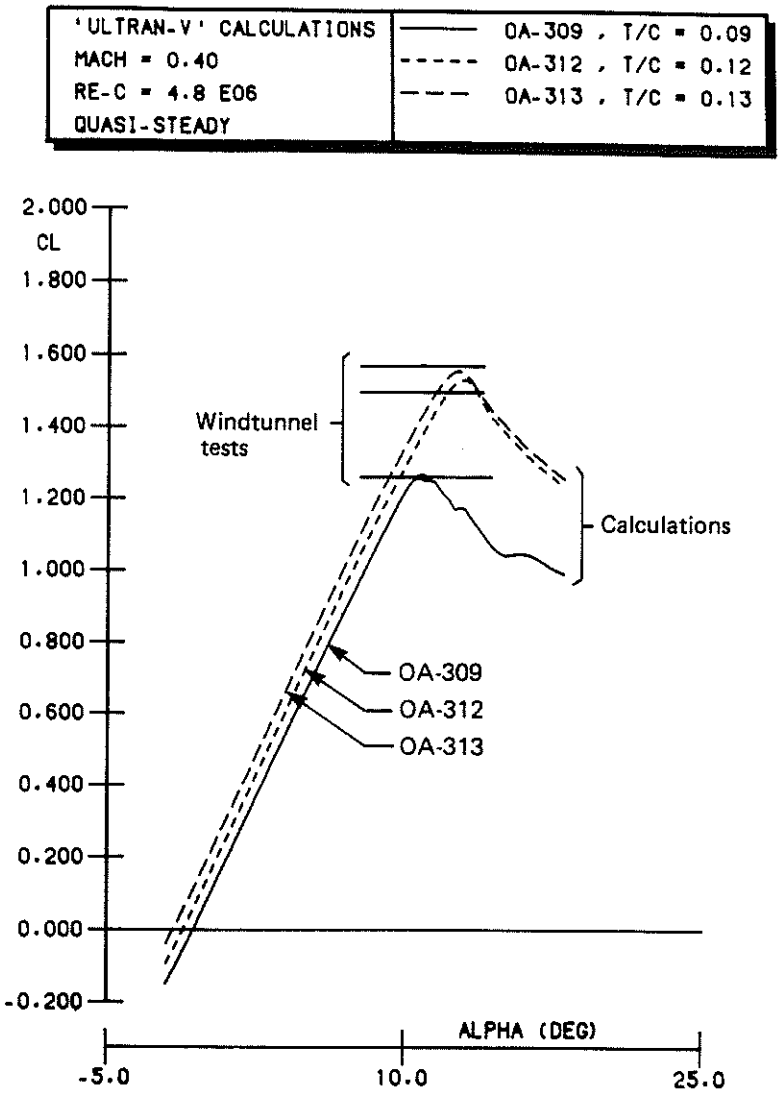

Fig. 6 Calculated lift curves

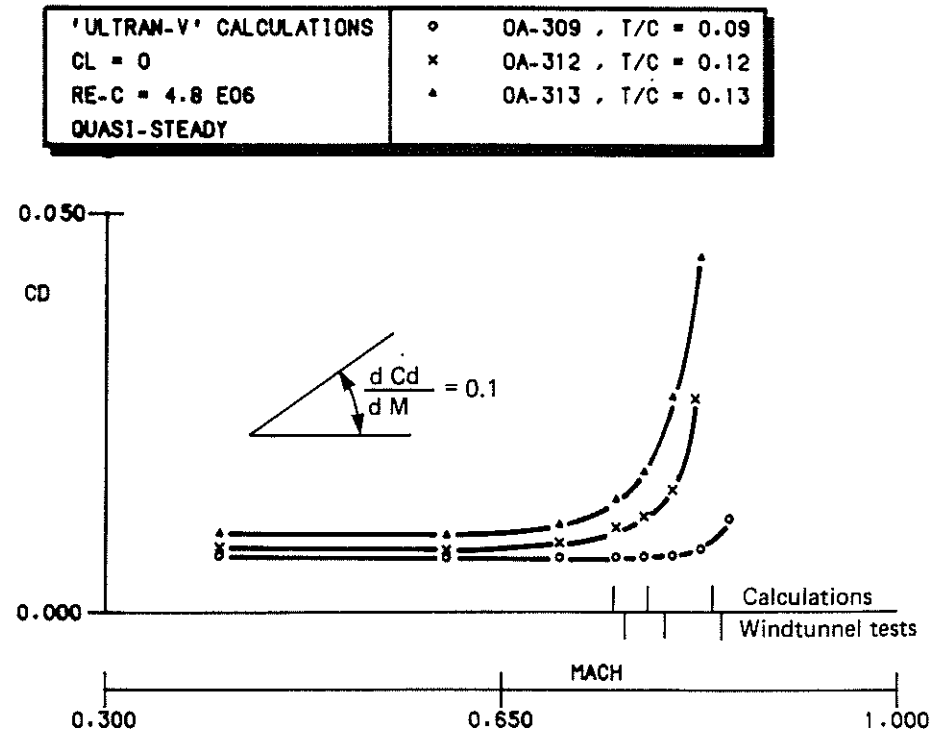

Fig. 7 Calculated drag curves showing drag-divergence mach number

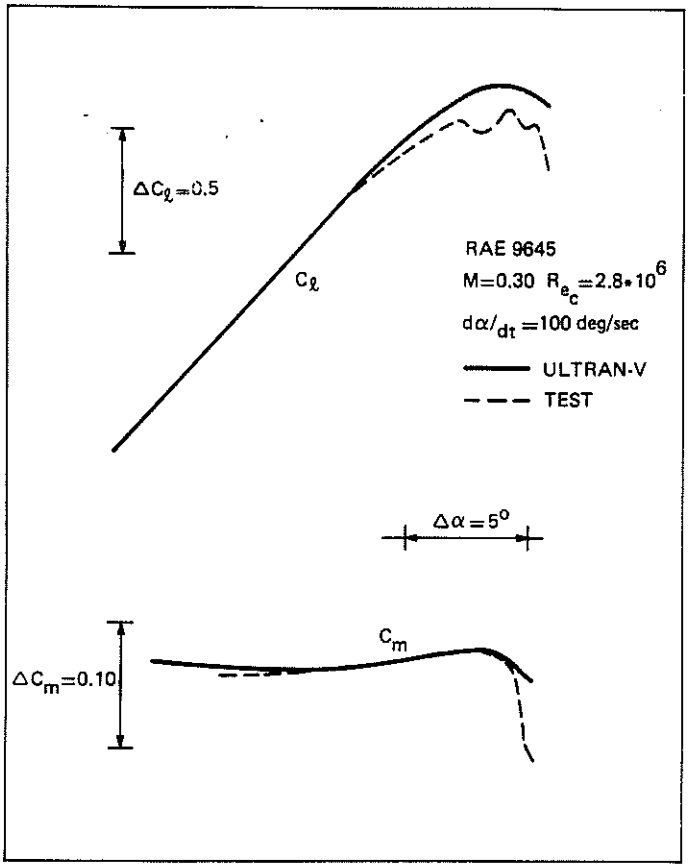

Fig. 8 Comparison of ramp data: low pitch rate

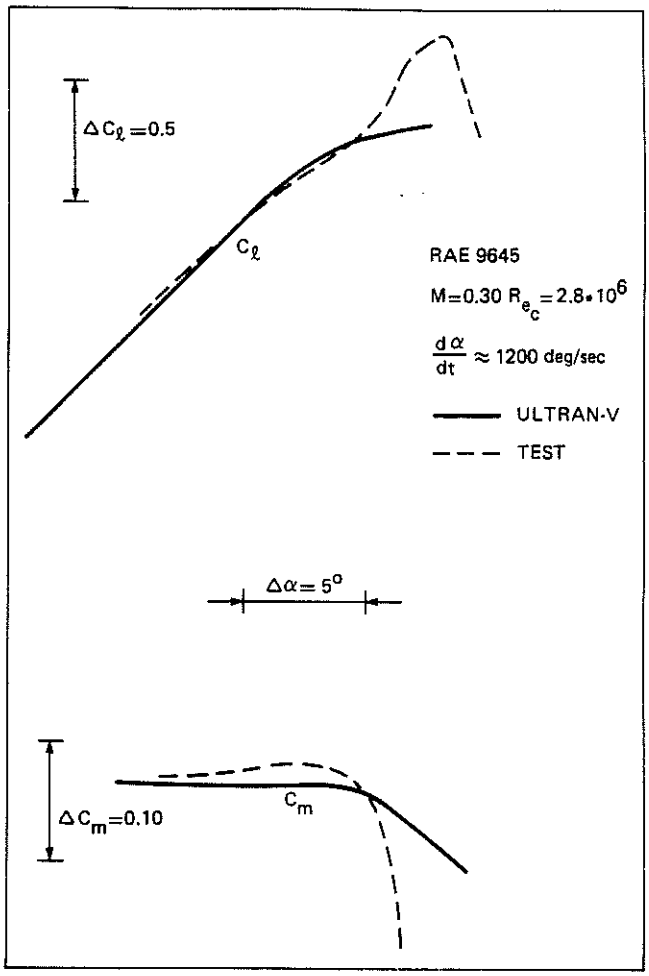

Fig. 9 Comparison of ramp data: high pitch rate

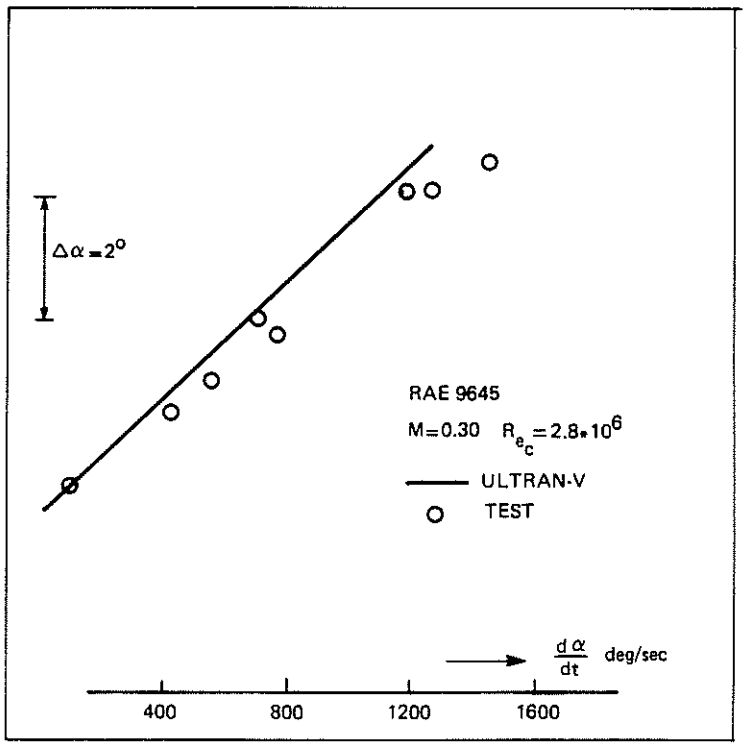

Fig. 10 Incidence for moment break (comparison of ramp data)